Using numerical simulations for estimating the influence of different parameters of long rod kinetic energy penetrators

Alan Catovic[1*], Faruk Razic[1]

[1] University of Sarajevo, Mechanical Engineering Faculty, Defense Technology Department, Bosnia

ABSTRACT

Simulations were performed with long rod kinetic energy penetrators to characterize important parameters used. Hohler & Stilp's experimental results served as the initial validation for the numerical model. Additionally, using numerical simulations, the impact of various (possible) penetrator materials on their penetration depth is illustrated. Additionally, the effects of using a steel jacket (sheath) over the penetrator and the penetrator fineness ratio (L/D) were examined. Research showed that the choice of penetrator material can significantly affect the penetrator's effectiveness. With a penetrator of depleted uranium alloy (0.75% titanium), the maximum penetration depth was attained. It was shown that when increasing the penetrator fineness, the increase in penetrator length has a large influence on penetration depth. Decreasing the penetrator diameter the penetration depth is also decreased. Numerical simulations also showed that to minimize penetration degradation, the penetrator jacket must be relatively thin.

Keywords:	Long rods, kinetic energy penetrator, numerical simulations, terminal ballistics

*Corresponding Author:

Alan Catovic
Defense Technology Department
University of Sarajevo
Vilsonovo setaliste 9, Bosnia
E-mail: catovic@mef.unsa.ba

1   Introduction

Long rod kinetic energy penetrators (such as the ones used in APFSDS - Armour Piercing Fin Stabilized Discarding Sabot munition) attract continual interest in the terminal ballistics community because of their high armor-piercing capabilities. With high muzzle velocities, large fineness ratio (L/D), and significantly higher densities than steel (hence large kinetic energy at the small impact area), they represent the highest threat for modern main battle tanks. Shaped charge projectiles are becoming less efficient against such targets because of composite and additional armor used and active protection system development (such as Trophy).

To some extent, this can be remedied by using top-attack mode projectiles (i.e., Javelin, NLAW - Next-generation Light Anti-tank Weapon), but APFSDS munition remains still the most potent anti-tank system today. Two materials are mainly used in kinetic energy penetrators, depleted uranium (DU) and heavy tungsten (W) alloys. DU alloys provide somewhat better penetration capabilities (albeit with reduced effects after the penetration).

Only a small number of countries have access to this material (made as a byproduct of the process of uranium enrichment). DU alloys are also pyrophoric but exhibit toxicity (in dispersed particle form) and radiation hazard. More details on the difference between these two materials can be found in [28].

In this paper, the emphasis will be on the numerical simulation method, where the influence of penetrator material on their efficiency will be investigated. Also, the influence of penetrator fineness and use of penetrator jacket will be investigated.

This research could help munition designers to better understand the use of certain materials (and their deficiencies) as penetrator material. Also, parameters of munition design, such as the application of steel jacket, can help designers to decide whether to use a jacket and what are the possible consequences.

2   Review of literature

Penetration dynamics parameters are presented in many books. Zukas [1] presents impact phenomena description, penetration mechanics, and material characterization, as well as different analytical, experimental, and numerical models. Walker [2] provides a very comprehensive treatment of impact and penetration mechanics. In [3], a penetration mechanics database is presented, with experimental tests from many researchers with different research objectives (armor and penetrator design & evaluation, space debris impact). The data are, generally, compiled in three distinct groups: a) perforation of finite-thickness targets, b) penetration into a semi-infinite target, and c) penetration after multiple impacts (for example, segmented rods).

Carlucci [4] gives a thorough overview of analytical and (semi)empirical penetration models for kinetic energy projectiles as well as an ammunition design practice.

Meyers [5] and Hazell [6] also provide the theory of penetration models for kinetic energy projectiles as well as considerations regarding numerical simulation methods. They also give an insight into material behavior during the penetration process. Penetration mechanisms are also given in [7], with an emphasis on materials consideration.

Rosenberg [8] provides penetration mechanics formulas, target defeat mechanisms description, experimental and numerical techniques, as well as material models for numerical simulations. Johnson [9] in his seminal book gives a detailed overview of stress wave theory, impulsive loading, and dynamic plastic deformation of material due to impact.

There are also many research papers regarding the terminal ballistics of kinetic energy penetrators. Held [10] gives a short tutorial on penetration models for KE penetrators for different velocities. The minimal impact energy for KE penetrators in RHA (Rolled homogeneous armour) targets was estimated by Lanz [11]; they concluded that by using high-strength sabots made of light materials and jacketed penetrators, one can obtain required penetration depths at lower kinetic energy values.

Frank [12] describes an optimum velocity that maximizes the kinetic penetrator performance for a given energy level. Keele [13] provides experimental data on the impact of a penetrator made of uranium alloy, with velocities of 1.7-2.4 km/s, on RHA targets. Comparisons are made with results obtained using tungsten alloy penetrators of identical size and L/D ratio.

Magness [14] provides an overview of recent studies on advanced penetrator materials, which include jacketed penetrators, amorphous and nanocrystalline alloys, adiabatic shearing tungsten composites, extreme deformation-treated WHAs (Wolfram Heavy Alloys), and uranium (U-V-X) alloys.

Rosset [15] gives an overview of new penetrator technologies (extending rods, cross-section and segmented penetrators, tandem rods, and sheathed penetrators), with a conclusion that implementing these concepts at any velocity poses a significant manufacturing challenge.

Three methods of approaching penetration mechanics are described by Wright [16]: engineering models, numerical simulation, and data correlation.

To determine the terminal ballistics characteristics of projectiles with kinetic energy, Auten [17] proposes the use of artificial neural networks. By shifting the computational complexity of the problem to the fitting (regression) phase of the algorithm, the speed of the method during analysis can be boosted relative to other terminal ballistic models. To predict the depth of penetration for eroding projectiles at impact velocities in the mechanical response regime of the materials, Riegel [18] showed how the Effective Flow Stress (EFS) strength model, which is based on empirical data, can be used as the average flow stress in the analytical penetration model.

In his work, Scheffler [19] examines the CTH hydrocode's capacity to predict the influence of the long rod nose geometry on the change from rigid body to eroding rod penetration for tungsten alloy rods that penetrate or perforate thick aluminum targets.

Rolled homogeneous armor (RHA) parameters are examined by Meyer [20]. The MIL-A-12560 (Military Standard for RHA) encompasses substantial variation in the material characteristics, depending on target plate thickness. The hardness can vary by more than 10%, even within a specific thickness specification.

With a cell size of 0.15 mm considered ideal, Park [21] simulated long-rod penetration in semi-infinite targets at velocities ranging from 500 to 3000 m/s using several mesh resolutions.

The relevance of the mentioned references is that some of them provide experimental data, such as [3], while some give valuable insight into the problem and possible directions of research. Some references, such as [12], offer advice on numerical simulations of this phenomenon.

3 Numerical simulations

3.1 Introduction

Ansys AUTODYN Lagrange processors were employed in the research for simulations. Time-dependent problems with geometric and material nonlinearities can be solved by hydrocode AUTODYN using finite-element, finite-difference, and finite-volume approaches.

Because the Lagrange formulation does not require the calculation of material transport across the mesh, it is computationally faster than the Eulerian method. Understanding free surfaces, history-dependent material behavior, and material interfaces is made easier by the Lagrange framework. The primary flaw in Lagrange's method is that excessive material movement can cause the numerical mesh to become severely distorted, producing an inefficient solution that may cause the computation to halt.

Additionally, AUTODYN provides additional approaches such as erosion to use the Lagrange formulation for severely distorted phenomena. The partial differential equations that need to be solved in the Lagrange processor express the conservation of mass, momentum, and energy in Lagrangian coordinates. These define the entire solution to the problem, along with a material model and a set of initial and boundary conditions [22].

3.2 Validation of the numerical model

The process of evaluating the uncertainty of a numerical model by comparison with test data is known as validation [23]. In this study, test data for the tungsten penetrator's penetration depth into the steel target were used to validate the numerical model in Ansys Autodyn. Hohler and Stilp's investigations provided the test results [3] (Table 1).

Test results, taken from [3], used in this section are valuable since not many countries can provide for such an expensive test. Also, specialized test equipment must be used in these tests. Besides that, not many countries have such a munition, so it is generally hard to find in the literature data that are useful in this regard.

Shock EOS (Equation of state) was utilized as the penetrator material in the simulations (table 2). One way to think of the Rankine-Hugoniot equations for shock jump conditions is as a relationship between any two of the following variables: particle velocity (up), pressure (p), energy (e), density (ρ), and shock velocity (U). Dynamic experiments revealed that there is an empirical linear relationship between these two variables for the majority of solids and many liquids across a broad range of pressure [22]:

$$U = c_0 + s u_p \tag{3.2.1}$$

Here s is the material constant that represents the U-u_p curve's slope and c_0 is the sound velocity for the particular material. Hugoniot's shock-based Mie-Gruneisen variant of the equation of state is:

$$p = p_H + \Gamma \rho \left(e - e_H \right) \tag{3.2.2}$$

with Γ representing coefficient of Gruneisen.

Hugoniot energy (e_H) and pressure (p_H) are expressed as:

$$e_H = \frac{1}{2} \frac{p_H}{\rho_0} \left(\frac{\mu}{1 + \mu} \right) \tag{3.2.3}$$

$$p_H = \frac{\rho_0 c_0^2 \mu (1 + \mu)}{[1 - (s - 1)\mu]^2} \qquad (3.2.4)$$

Here $\mu = (\rho/\rho_0) - 1$.

Table 1. Parameters from Hohler and Stilp experimental data [3]

	1. Test	2. Test	3. Test	4. Test	5. Test
Impact data					
Velocity (m/s)	992	1025	1373	1487	1570
Yaw angle (°)	<1				
Results					
P (mm) - penetration depth	21.6	24.4	47.5	56.7	64
d (mm) - entry hole diameter	10.9	11	12.2	12.5	12.9
P/L	0.36	0.407	0.792	0.945	1.067
Penetrator data					
L (mm)	60				
D (mm)	6				
L/D	10				
Material	W (tungsten)				
ρ (kg/m³)	19300				
Nose	Flat				
Hardness (BHN)	433				
Elongation (%)	0.15				
Target data					
Material	HzB,A steel				
ρ (kg/m³)	7850				
Hardness (BHN)	255				

The target material was treated with a linear EOS. P is a function of particular volume (v) and specific entropy (S) in the ideal gas equation. An alternative method is to examine the initial elastic behavior, which is represented by the following approximation to Hooke's Law: [22]:

$$p = K\mu \qquad (3.2.5)$$

Here K is the bulk modulus of the material and $\mu = (\rho/\rho_0) - 1$.

In order to model the strength effects, the elastic limit and transition to plastic flow for the penetrator were described using the Von Mises yield criterion [22].

During the validation procedure, the target material's strength effects were modeled using the Johnson-Cook model. The yield stress Y is defined by the model as [22]:

$$Y = [A + Be_p^n][1 + Clog e_p^*][1 - T_H^m] \qquad (3.2.6)$$

Here: e_p is plastic strain, e_p^* is plastic strain rate, and T_H is homologous temperature. A (yield stress), B (hardening constant), C (hardening exponent), n (strain rate constant), and m (thermal softening exponent) are the material constants listed in Table 2.

Steel 4340 is the main material selected for the target in numerical simulations (this material can be taken as an adequate substitution [18] for steel HzB,A from experiment - see Table 1), and for the penetrator - tungsten (W), with parameters adopted from the AUTODYN material library. These parameters are shown in detail in Table 2.

Table 2. Materials parameter data used in simulations (AUTODYN library)

Shock EOS - penetrator					
Material	ρ (g/cm^3)	Gruneisen coeff.	c_0 (m/s)	s	Spec.heat (J/kgK)
Tungsten (W)	19.3	1.58	4000	1.268	0
Linear EOS data - target					
Material	ρ (g/cm^3)	Bulk modulus (kPa)	Reference Temperature (K)	Specific heat (J/kgK)	Thermal Conductivity (J/mKs)
Steel 4340	7.85	$1.59 \cdot 10^8$	300	477	0

Von Mises strength model - penetrator		
Material	Shear modulus (kPa)	Yield Stress (kPa)
Tungsten (W)	$1.6 \cdot 10^8$	$2 \cdot 10^6$

Johnson-Cook strength model - target							
Material	Shear modulus (kPa)	Yield stress (kPa)	Hardening constant	Hardening exponent	Strain rate constant	Thermal softening exponent	Melting temp. (K)
Steel 4340	$8.18 \cdot 10^7$	$7.92 \cdot 10^5$	$5.1 \cdot 10^5$	0.26	0.014	1.03	1793

Geometric parameters of the KE penetrator and target in the numerical simulation model are presented in Fig. 1 (see also Table 1).

A 2D axisymmetric analysis was performed, with the initial condition - impact velocity of the penetrator (taken from experimental tests, Table 1).

On the target outer border, a fixed displacement boundary condition was applied.

Parts were defined as Lagrangian, with a mesh element size of 0.125 mm (recommended by many authors, i.e. in [21]). Mesh for the target was graded in the J direction (Fig. 2), making the simulation run faster than using uniform mesh.

In the graded mesh (target), the same-size smaller elements (the same as for the penetrator) were chosen in the penetration zone of interest (the size of this zone is 2D, where D is penetrator diameter).
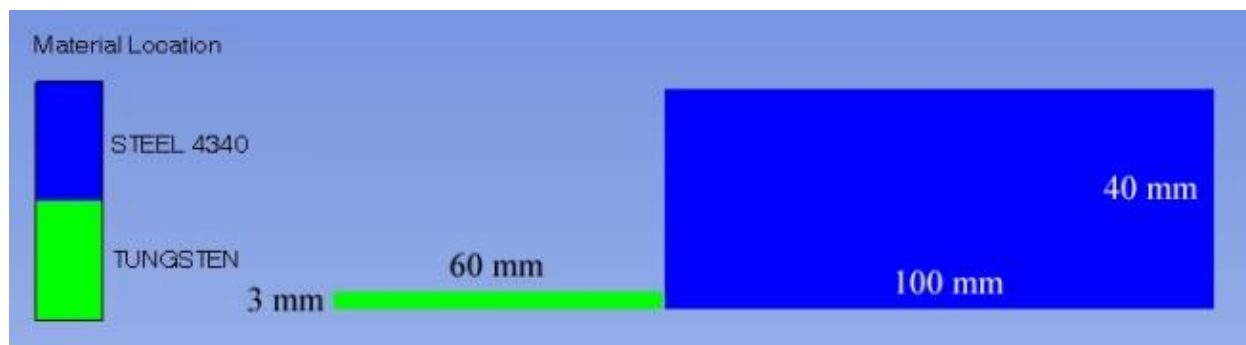

Figure 1. Geometric parameters of penetrator and target in 2D numerical model

Interaction type between both Lagrangian parts was chosen as the default Lagrangian/Lagrangian - External gap option. The erosion type, used in numerical simulations, was specified as instantaneous geometric strain with a default value of 1.5 (150%) for both parts (these erosion values are recommended also in reference [24]).

Results of simulations and comparison with available experimental data are presented in Table 3. Relative difference values were determined as $rel_{dif} = (value - value_{ref})/(value_{ref})$. In these simulations, impact velocities were given in Table 3, the angle of impact was 0° (normal impact angle), and these conditions were kept constant.
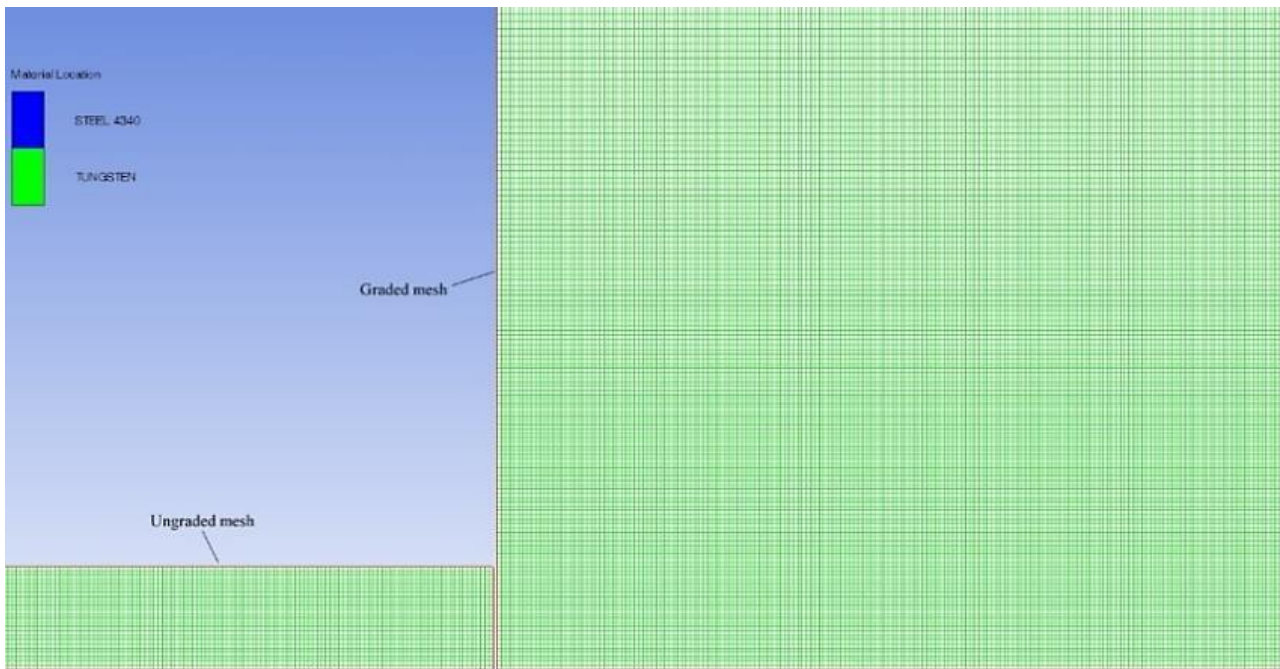
Figure 2. Grading of mesh for target

As can be seen, simulation results closely match experimental data, regarding penetration depth (P) and radius of entry hole crater (r).

Table 3. Results of simulations and comparison with experimental data (validation of a numerical model)

Test	V (m/s)	P_{exp} (mm)	P_{simul} (mm)	Rel. diff. for P (%)	r_{exp} (mm)	r_{simul} (mm)	Rel. diff. for d (%)
1	992	21.6	22.91	6.06	5.45	5.14	6.03
2	1025	24.4	24.5	0.41	5.5	5.32	3.38
3	1373	47.5	47.82	0.67	6.1	6.17	1.15
4	1487	56.7	55.5	2.16	6.25	6.4	2.4
5	1570	64	60.7	5.43	6.45	6.7	3.86

Penetration holes and total penetration depths, obtained using performed numerical simulations, are visually presented in Fig. 3, for different impact velocities of the penetrator, with all other numerical parameters beeing the same.

3.3 Influence of penetrator material on penetration depth

Materials used in the simulation correspond to potential materials with higher density and are based on tungsten and depleted uranium alloys. Results were compared with the original penetrator from tungsten (density 19,3 g/cm^3), presented in the previous section, with an impact velocity of 1487 m/s (Test 4, Table 1). Except a few differences due to differing penetrator materials, all of the numerical setup settings for the simulations were the same as those shown in the validation section (section 3.2).

Tables 4, 5, and 6 (Shock EOS, Steinberg-Guinan model, Johnson-Cook model) provide parameters of penetrator materials that are utilized in numerical simulations to ascertain the influence of materials on the penetration depth into the steel target. See [25] for further information on the Steinberg-Guinan strength model.

Steel 4340 is the main material used for the target, and the AUTODYN material library's original specifications were used (Table 2). A linear EOS and Johnson-Cook model was used for modeling the target material and one of the penetrator variants (Table 2) which was used to compare higher-density materials with steel performance (it is known that some older Soviet kinetic energy penetrators for APFSDS munition were made of steel).
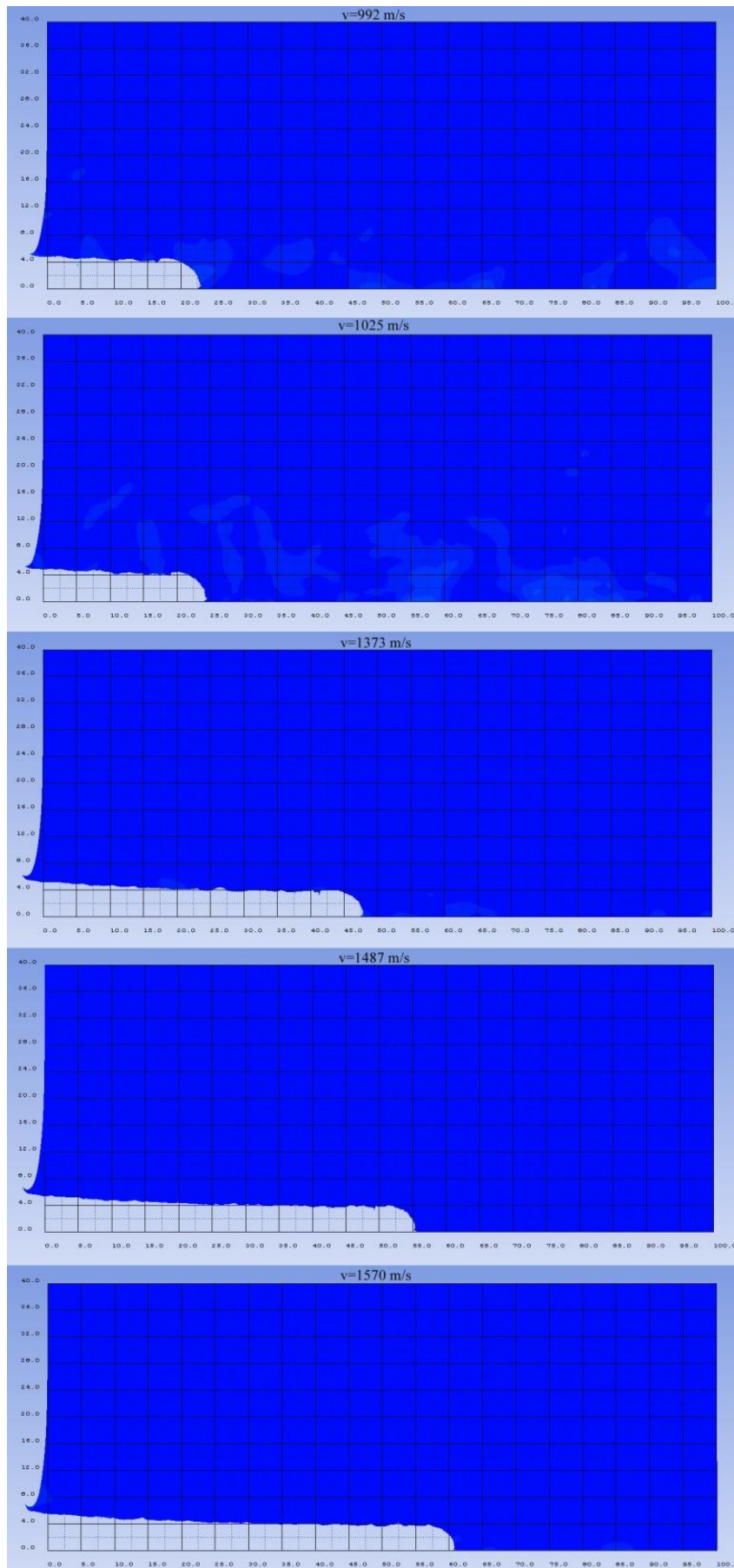
Figure 3. Penetration holes and total penetration depths, obtained by numerical simulations using different impact velocities (validation of the 2D numerical model)

Table 4. Shock EOS data for various penetrator materials (AUTODYN material library) utilized in simulations

Penetrator material	ρ (g/cm³)	Gruneisen coeff.	c_0 (m/s)	s	Spec. heat (J/kgK)
W4Ni2Fe	18.167	1.67	4030	1.237	143
W alloy	17.00	1.54	4029	1.237	134
U.75Ti	18.62	2.32	2567	1.619	111
U5Mo	18.17	2.32	2590	1.56	114
U8Nb3Zr	16.45	1.90	2570	1.50	113

Table 5. Penetrator materials' Steinberg-Guinan strength model parameters (AUTODYN material library)

Material	Shear modulus (kPa)	Yield stress (kPa)	Max. yield stress (kPa)	Hardening constant	Hardening exponent	Derivative dG/dP	Derivative dG/dT (kPa/K)	Derivative dY/dP	Melting temp. (K)
W4Ni2Fe	$1.45 \cdot 10^8$	$1.87 \cdot 10^6$	$4 \cdot 10^6$	7.7	0.13	1.494	$-2.204 \cdot 10^4$	0.01926	$2.263 \cdot 10^3$
U.75Ti	$7.4 \cdot 10^7$	$9.5 \cdot 10^5$	$2.2 \cdot 10^6$	1000	0.095	4.351	$-5.802 \cdot 10^4$	0.05586	$1.71 \cdot 10^3$
U5Mo	$3.5 \cdot 10^7$	$8.5 \cdot 10^5$	$1.68 \cdot 10^6$	250	0.25	1.201	$-1.001 \cdot 10^4$	0.02916	$1.82 \cdot 10^3$
U8Nb3Zr	$2.33 \cdot 10^7$	$1.6 \cdot 10^6$	$1.6 \cdot 10^6$	0.0	0.0	0.8505	$-6.011 \cdot 10^3$	0.05840	$1.42 \cdot 10^3$

Table 6. Parameters of the Johnson-Cook strength model for penetrator material (AUTODYN library)

Material	Shear modulus (kPa)	Yield stress (kPa)	Hardening constant	Hardening exponent	Strain rate constant	Thermal softening exponent	Melting temp. (K)
W alloy	$1.6 \cdot 10^8$	$1.506 \cdot 10^6$	$1.77 \cdot 10^5$	0.12	0.016	1.00	1723

Important data derived from numerical simulations are displayed in Tab. 7. These include the penetration depth, penetration hole radius, penetration depth percentual decline relative to the original penetrator (tungsten), and a ranking of possible materials based on the penetration depth. A depleted uranium alloy (with 0.75% titanium) penetrator produced the maximum penetration depth in the simulations that were run: P=55.61 mm, which is a 0.2% increase compared to the original penetrator from tungsten (55.5 mm). The lowest penetration depth (P=22.17 mm; 150.34% decrease compared to the original penetrator from tungsten) was achieved with a steel penetrator. More specifics and details on these materials can be found in our earlier research [25].

Table 7. Parameters derived from numerical simulations, where materials are ranked according to penetration depth findings

Penetrator material type	Entry hole radius (mm)	Penetration depth (mm)	Penetration depth increase/decrease compared to orig. penetrator (tungsten)	Ranking of materials based on penetration depth
W4Ni2Fe	6.53	49.91	11.20% (decrease)	**4**
W alloy	6.37	53.63	3.49% (decrease)	**2**
U.75Ti	6.46	55.61	0.20% (increase)	**1**
U5Mo	6.53	52.83	5.05% (decrease)	**3**
U8Nb3Zr	6.38	49.73	11.60% (decrease)	**5**
Steel 4340	6.62	22.17	150.34% (decrease)	**6**

3.4 Influence of penetrator fineness on penetration depth

The influence of penetrator fineness (L/D) on penetration depth was analyzed. As a penetrator material, depleted uranium alloy U.75%Ti was used, with density of 18.62 g/cm³. The parameters of this material are presented in Section 3.3. The setup in simulation was the same as in the previous section, with variations related to different penetrator fineness and increasing the length of the target (a larger P was expected). The

fineness ratio in simulations was 10-25, with first penetrator diameter held constant (Table 8) and then penetrator length held constant (Table 9). The original configuration relates to the penetrator with L/D=10, where L=60 mm and D=6 mm. The penetration depth for this configuration was 55.61 mm (Table 7).

Table 8. Variation in penetration depth (P) for different penetrator fineness (L/D); penetrator was constant

L/D ratio	L (mm)	D (mm)	P_{simul} (mm)	Rel. diff. compared to original config. (%)
10	60	6	55.61	original config.
15	90	6	78.44	41.05
20	120	6	101.23	82.04
25	150	6	126.25	127.03

Table 8. shows that, when increasing the penetrator fineness (when D=const), the increase in penetrator length has a large influence on penetration depth. For example, by increasing the penetrator length by 150% (from 60 mm to 150 mm, thus increasing the penetrator fineness from 10 to 25), the penetration depth is increased by 127%.

Table 9 shows the influence of kinetic energy penetrator diameter on its penetration depth (when penetrator length is held constant throughout). Decreasing the penetrator diameter by 100% (from 6 mm to 3 mm, thus increasing the penetrator fineness from 10 to 25), the penetration depth is decreased by 9.55%.

Table 9. Variation in penetration depth for different penetrator fineness (L/D); penetrator length constant

L/D ratio	L (mm)	D (mm)	P_{simul} (mm)	Rel. diff. compared to original config. (%)
10	60	6.00	55.61	original config.
15	60	5.00	53.79	3.38
20	60	4.00	52.54	5.84
25	60	3.00	50.76	9.55

3.5 Influence of penetrator jacket on penetration depth

The influence of the penetrator jacket (case, sheath) on penetration depth was also analyzed, using numerical simulations. The material for the penetrator was U.75%Ti and steel 4340 was used as a jacket and target. Unlike carbon-fiber-reinforced plastic, the steel jacket maintains greater contact with the penetrator core and does not fall off [27]. Parameters of materials are presented earlier in Tables 2, and 4-6.

Table 10 Variation in penetration depth for different penetrator jacket thickness (t); penetrator fineness constant

L/D ratio	L (mm)	D (mm)	t (mm)	t/D ratio	P_{simul} (mm)	Rel. diff. compared to original config. (%)
10	60	6	0	0	55.61	original config.
10	60	6	0.25	0.04	53.68	3.47
10	60	6	0.5	0.08	51.48	7.43
10	60	6	1	0.17	44.35	20.25
10	60	6	1.5	0.25	37.7	32.21

Numerical simulations showed (Table 10) that - to minimize penetration degradation - the jacket thickness (t) must be relatively small, in the order of t/D<0.05. For example, when t/D=0.04, penetration depth was reduced by 3.5% (Table 10). In general, jackets help long-rod penetrators since they increase their stiffness under flexure, which is helpful in launch conditions when higher accelerations are feasible. However, this research proved that the thickness of the jacket shouldn't go above a specific value to avoid the possibility of a decreased penetration capability. Fig. 4 shows different times of the penetration process (material location) for the sheated penetrator with a theoretical case thickness of 0.5 mm.
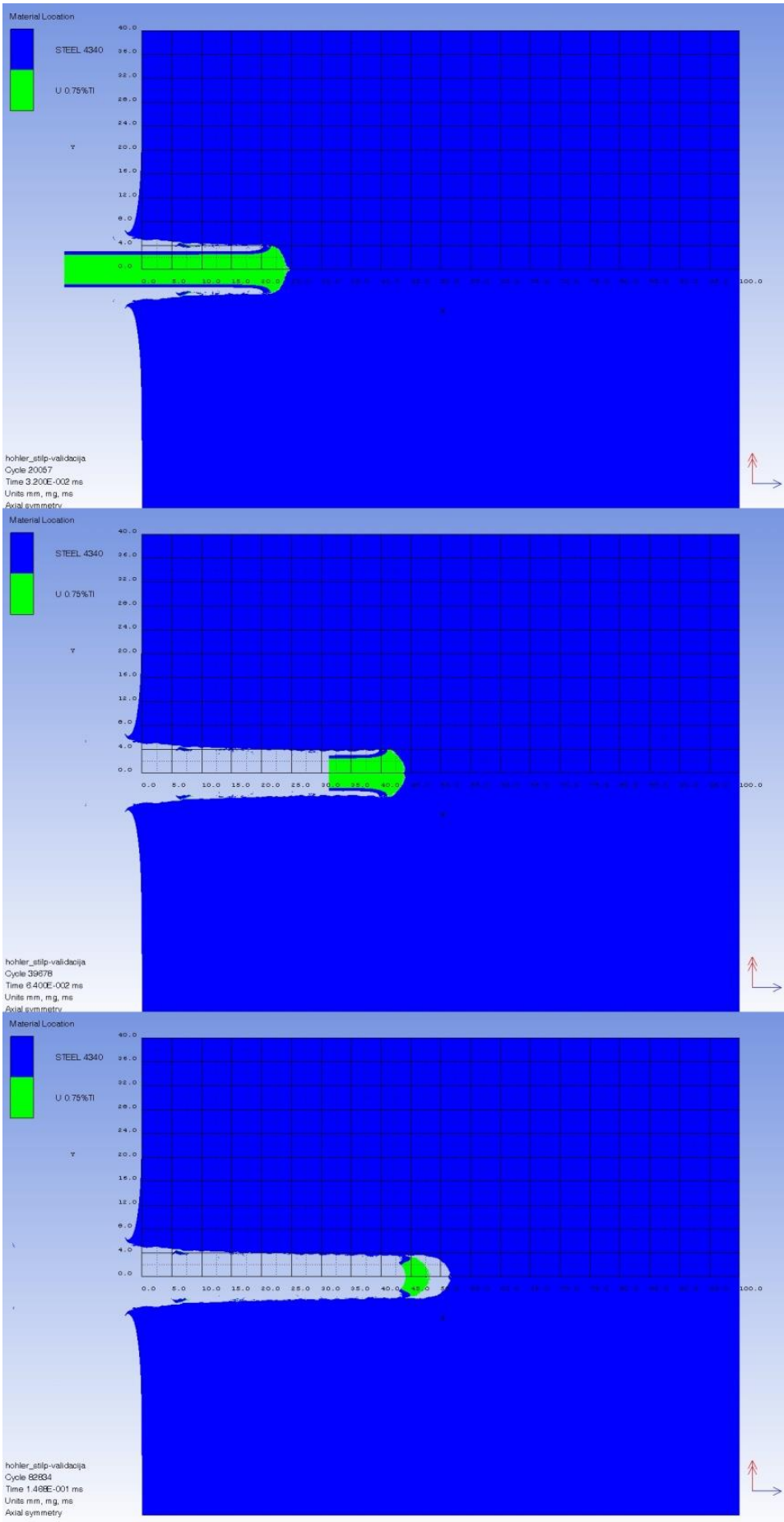
Figure 4. Different times of penetration process for case penetrator

4 Conclusions

Numerical simulations using the Ansys AUTODYN were used to determine the effect of different penetrator materials and their geometry on the penetrating capabilities into a steel target. Research has shown that the choice of penetrator material can significantly affect the penetrator's effectiveness. With a penetrator composed of depleted uranium alloy with 0.75% titanium, the maximum penetration depth was attained. Materials were chosen from the AUTODYN material library. Any new material planned to be used in simulations should go through a detailed characterization process using dynamic impact experiments. It was confirmed that when increasing the penetrator fineness (when D=const), the increase in penetrator length has a large influence on penetration depth. Namely, by increasing the penetrator length by 150% (increasing the penetrator fineness from 10 to 25), the penetration depth is increased by 127%. Decreasing the penetrator diameter by 100 % (thus increasing the penetrator fineness from 10 to 25 when L is held constant), the penetration depth is decreased by around 9.5%. Numerical simulations also showed that to minimize penetration degradation, the penetrator jacket (sheath, case) must be relatively thin (in the order of $t/D < 0.05$). So, even though the jacket is useful during the projectile launch process, care must be taken to choose a not overly thick case, which is in accordance with other authors' conclusion [26].

An overall design optimization procedure for kinetic energy penetrators can be the focus of future investigation, involving here mentioned parameters, and also additional design parameters (i.e. upscaling of the geometry, optimizing penetrator frontal part, possible use of novel technologies, etc. Novel technologies, such as extending rods, cross-section, and segmented penetrators. Regarding extending rods, the general idea is to launch a penetrator in a compact state and then extend it in flight, preferably near the target. Penetrators with cross-sections different from a solid circle have been designed with examples such as triform and cruciform cross-section rods with a baseline circular cross-section. The general segmented rod concept is to have a long string of low LTD rods hit the target sequentially at the same point. The fundamental advantage of segmented rod penetrators is that, theoretically, they are not limited in penetration depth at high velocity to the classic density law. Using numerical simulations researchers can significantly reduce munition design time and save money in the process.

References

[1] J. Zukas, *High Velocity Impact Dynamics*. New York: Wiley Interscience, 1990, ISBN 978-0471514442.

[2] D. J. Walker, *Modern Impact and Penetration Mechanics*. Cambridge University Press, 1st edition, 2021, ISBN 978-1108497107.

[3] C. E. Anderson, B. L. Morris, and D. L. Littlefield, *A Penetration Mechanics Database*. San Antonio: Southwest Research Institute, 1992.

[4] D. E. Carlucci, and S. S. Jacobson, *Ballistics - Theory and Design of Guns and Ammunition*. Boca Raton: CRC Press, 2007, ISBN: 978-1-4200-6618-0.

[5] M. A. Meyers, *Dynamic Behavior of Materials*. New York: John Wiley & Sons, 1994, ISBN: 0-471-58262-X.

[6] P. J. Hazell, *Armour*. Boca Raton: CRC Press, 2016, ISBN: 978-1-4822-3830-3.

[7] National Materials Advisory Board, *Opportunities in Protection Materials Science and Technology for Future Army Applications*. Washington: The National Academies Press, 2011, ISBN: 978-0-309-21285-4.

[8] Z. Rosenberg, and E. Dekel, *Terminal Ballistics*, 3rd Edition, Springer Nature Switzerland AG, 2020, ISBN: 978-3-030-46611-4.

[9] W. Johnson, *Impact Strength of Materials*. London: Edward Arnold, 1972, ISBN: 0713132663.

[10] M. Held, "A Tutorial on the Penetration of Kinetic Energy (KE) Rounds," *Journal of Battlefield Technology*, vol. 7, no. 1, 2004, ISSN 1440-5113.

[11] W. Lanz, and W. Odermatt, "Minimum Impact Energy For KE-Penetrators In RHA-Targets," in *European Forum on Ballistics and Projectiles*, French-German Research Institute of Saint-Louis - France, April 2000. Available: https://apps.dtic.mil/sti/pdfs/ADA385710.pdf

[12] K. Frank, and J. A. Zook, "Energy-efficient Penetration of Targets," Report BRL-MR-3885, Ballistic Research Laboratory, Aberdeen Proving Ground, Maryland, 1991.

[13] M. J. Keele, E. J. Rapacki, and W. J. Bruchey, "High Velocity Performance of a Uranium Alloy Long Rod Penetrator," Report BRL-TR-3236, Ballistic Research Laboratory, Aberdeen Proving Ground, Maryland, 1991.

[14] L. Magness, "Advanced Penetrator Materials," in *Proceedings from Armaments for the Army Transformation Conference*, Parsippany NJ, 2001. Available: https://apps.dtic.mil/sti/pdfs/ADA393800.pdf

[15] W. S. Rosset, "An Overview of Novel Penetrator Technology," Army Research Laboratory, Aberdeen Proving Ground, Maryland, 2001. Available: https://apps.dtic.mil/sti/pdfs/ADA387329.pdf

[16] T. W. Wright, and K. Frank, "Approaches to Penetration Problems," Technical Report BRL-TR-2957, Ballistic Research Laboratory, Aberdeen Proving Ground, Maryland, 1998.

[17] J. R. Auten, and R. J. Hamell, "Predicting the Terminal Ballistics of Kinetic Energy Projectiles Using Artificial Neural Networks," in *Proceedings of the Conference for Information Systems Applied Research*, San Antonio, Texas, USA, 2013, ISSN: 2167-1508.

[18] J. P. Riegel, and D. Davison, "Consistent constitutive modeling of metallic target penetration using empirical, analytical, and numerical penetration models," *Defence Technology*, vol. 12, no. 2, pp. 201-213, 2016, ISSN: 2214-9147.

[19] D. R. Scheffler, "CTH Hydrocode predictions on the effect of rod nose-shape on the velocity at which tungsten alloy rods transition from rigid body to eroding penetrators when impacting thick aluminium targets," in *Transactions on the Built Environment*, WIT Press, 1996, vol. 22, ISSN: 1743-3509.

[20] H. W. Meyer Jr., and D. S. Kleponis, "An analysis of parameters for the Johnson-Cook strength model for 2-in-thick Rolled Homogeneous Armor," Technical Report ARL-TR-2528, Army Research Laboratory, Aberdeen, Maryland, 2001. Available: https://apps.dtic.mil/sti/citations/ADA392414

[21] B. Y. Park, R. B. Leavy, and J. H. J. Niederhaus, "Penetration of rod projectiles in semi-infinite targets: a validation test for Eulerian X-FEM in ALEGRA," Sandia Report 2013-1863, Sandia National Laboratories, Albuquerque, New Mexico, 2013. Available: https://www.osti.gov/biblio/1088058

[22] *AUTODYN® - Explicit Software for Nonlinear Dynamics, Theory Manual - Revision 4.3*, Century Dynamics Inc., 2005.

[23] J. Tu, G. H. Yeoh, and C. Lie, *Computational Fluid Dynamics - A Practical Approach*, 3rd Edition, Butterworth-Heinemann, 2018, ISBN 978-0081011270.

[24] E. Galuta, and W. REGIG, "Numerical simulations of RC panels subjected to high-speed projectile - Erosion selection in AUTODYN-3D code," *IJISET - International Journal of Innovative Science, Engineering & Technology*, vol. 4, no. 8, 2017, ISSN 2348-7968.

[25] A. Catovic, "Research of influence of different shaped charge liner materials on penetration depth using numerical simulations," *Periodicals of Engineering and Natural Sciences*, vol. 11, no. 4, 2023, ISSN: 2303-4521.

[26] B. R. Sorensen, K. D. Kimsey, J. A. Zukas, and K. Frank, "Numerical analysis and modeling of jacketed rod penetration," *International Journal of Impact Engineering*, vol. 22, pp. 71-91, 1999, ISSN 1879-3509.

[27] H. F. Lehr, E. Wollman, and G. Koerber, "Experiments with jacketed rods of high fineness ratio," *International Journal of Impact Engineering*, vol. 17, pp. 517-526, 1995, ISSN 1879-3509.

[28] A. Gsponer, *Depleted-Uranium Weapons: The Whys and Wherefores*. Independent Scientific Research Institute, Geneva, Switzerland, 2008. Available: https://arxiv.org/pdf/physics/0301059.pdf